Strojniški vestnik - Journal of Mechanical Engineering 65(2019)3, 161-180
DOI:10.5545/sv-jme.2018.5788
Original Scientific Paper
Received for review: 2018-10-11
Received revised form: 2019-01-23
Accepted for publication: 2019-01-28
© 2019 Journal of Mechanical Engineering. All rights reserved.

Active Structural Derivator in the Design Crystallization Phase of L7e Vehicle Structures

Roman Pawel Jedrzejczyk* – Michael Sigmar Alb
Virtual Vehicle Research Center, Austria

Over the past years, engineers have begun to apply topology optimization (TO) to obtain the first design proposals for new structures. Consequently, designers need to transform the bionic shapes of the TO results into manufacturable geometry that employs the available body-in-white structure types (BSTs) and affirms the efficient and suitable lightweight design. The lack of standardized methodologies, however, forces designers to transform the bionic shapes of the TO subjectively, which results in insufficient and inadequate design proposals. Many different separate geometrical transitions that attempt to transform the TO results into the one of the selected BSTs make the design process even more difficult to manage. For this reason, we have proposed the active structural derivator (ASD) as an extension of our existing integrative CAE-driven design process (ICDDP). The ASD allows for the smooth transition of the TO results and the practical assessment of the selected BSTs such as tubular space frame, space frame, hybrid structure, unibody and monocoque. Our ASD simultaneously employs the size and free-size optimizations under the specific steering criteria within one simulation model, which consists of fundamental engineering-based geometry (beams and plates), to generate the design concepts of the different BSTs for given sets of different requirements. We present the results of our ASD for the new structure of an electrified eQuad vehicle that reveal the ASD's ability to select, allocate and optimize various beam types (arbitrary and defined) together with the plate (shell) geometry. The results assert that the ASD enables engineers to deliver new applicable and lightweight structures.

Keywords: bionic geometry, body-in-white, design process, FEM, free-size optimization, ICDDP, topology optimization, size optimization, vehicle structure design

Highlights

- *ASD makes possible the smooth transition of the TO results into one of the selected BSTs.*
- *ASD assesses the load-bearing characteristics such as compression-tension, bending and torsion of these structures.*
- *ASD entitles designers to direct comparisons between the various obtained designs of the BSTs and indicates the loads (load cases) with the highest compliance (inverted structural stiffness).*
- *ASD permits the calculations for composite materials and system identifications.*

0 INTRODUCTION

In recent years, the mechanical engineering industry has experimented with methods that unify a systematic approach to the design process and support of computer-aided-engineering (CAE) tools. These methods mainly utilize topology optimization (TO) in many development studies of new structures **[1]** and **[2]**. As a result, the TO delivers bionic shapes of new structures that need to be translated into manufacturable geometry. This transition from a bionic model to geometric solutions has not been fully defined because the bionic shapes challenge a coherent and qualitative interpretation **[3]**. Such interpretation should take full advantage of reasoning material application **[4]**, which is suggested by the TO results. Consequently, the transition of bionic shapes to a new structure can be performed by employing three-dimensional (3D) printing technologies **[5]** or by deriving a new structure from the bionic results that is traditionally manufactured.

New lightweight structures can now be printed out in various 3D printers for different material types, including metal alloys **[5]** and **[6]**. Such manufacturing processes offer an opportunity to examine a functional prototype earlier, check a proper design accurately and bring a final product faster to the market **[7]**. Additionally, rapid manufacturing methods deliver spare parts for unique mechanisms as well as demonstrators for new product ideas **[6]**. Although the usage of 3D printing technologies is growing rapidly, these technologies also have downsides **[6]** and **[7]** such as necessary additional preparation of bionic geometry for 3D printers, high costs of metallic powders, expensive small dimensional 3D printers, inferior geometric dimensioning and tolerancing. Moreover, 3D printing is improper for structures that exhibit modular scalable constructions (e.g. automotive industry). These facts limit the practical applications of 3D printing technologies to narrow manufacturing areas.

The bionic model can also be transitioned into a traditionally manufactured structure. This transition,

*Corr. Author's Address: Virtual Vehicle Research Center, Inffeldgasse 21a, 8010 Graz, Austria, RomanPawel.Jedrzejczyk@v2c2.at

however, is subjective because designers and engineers interpret the bionic shapes by assessing the TO results individually. In consequence, designers and engineers need to develop one or select from a few unstandardized methods [8] to perform the bionic shapes' transition reasonably. Thus, the new developed structures exhibit a poor and inadequate lightweight design.

1 ACTIVE STRUCTURAL DERIVATOR

1.1 Designing Vehicle Structures

Engineers derive a new vehicle structure from a bionic model by applying selected body-in-white structure types (BSTs). This approach can privilege or even restrict lightweight design of new structures frequently [9]. Recent studies have exemplified that specific BSTs favor lightweight design more than others [9] to [12]. A body-in-white (BIW) of a mid-range sedan, for example, has the same weight (ca. 188 kg) for an aluminum space frame and an aluminum unibody; however, the capable production volumes and possible production costs are significantly different, thus restricting an aluminum space frame BST to low production volumes.

Not only improper applied BSTs can be expensive. Omitting the pieces of a new structure that was insufficiently translated from the TO results into a geometrical engineering model influences the load-bearing capabilities of such structures crucially. To enhance a newly designed structure, engineers apply extra structural optimization [13] and [14] design steps, consequently increasing the overall product development duration.

To target the individual needs of new vehicle customers more directly [15], the number of model derivatives offered by vehicle manufacturers has increased markedly. Designers should assess whether or not a design of model derivatives matches new specifications [16] and [17] by carrying out extra analyses (e.g. system identification). In addition, the 18-month development cycles restrict a number of feasible design studies for a new structure to only a few [18]. Thus, possible lightweight actions of a new design such as new material types, different BSTs and sandwich material types are expensive to apply in the later phase of the development process, which influences the final price of new vehicles [19].

Optimization technologies support the development process notably [20] and [21], but the lack of rapid method-ology to analyze available BSTs for a new vehicle model and almost 40 different CAE tools present in the automotive industry [8] hinder possible cost estimations of such technologies' introductions to a current development and handicap engineers to distinguish between the suitable BSTs that are equal to the lightweight design yet challenging in production know-how [22] and [15]. Moreover, engineers demand that an innovative method selects, allocates and optimizes fundamental structural elements (beams and plates) within one simulation model and allows for fast geometrical updates and the modulization of similar structures [22].

For these reasons, the design method that allows engineers to transform the bionic shapes into geometrical engineering-based models is presented in this paper. Our active structural derivator (ASD) enables designers to reveal the omitted extra details of the translated geometry so that their presence in a new structure can be further analyzed and optimized during the execution of the ASD. The term derivator, in fact, is adopted from mathematics, where it serves to refine and in a certain sense simplify the theory of homotopical algebra [23]. The ASD permits engineers to investigate various configurations of the BSTs such as tubular space frame, space frame, unibody, hybrid structure and monocoque for a new vehicle structure. For the various configurations of the different structure types, the ASD enables designers to assess several arrangements of diverse materials such as isotropic and orthotropic (e.g. steel, aluminum, composites and sandwich composites).

The ASD also offers a possibility to select, allocate and optimize the fundamental structural elements (beams and plates) for a newly designed structure. This method distinguishes between assorted types of beam cross-sections such as arbitrary and defined (e.g. box, rod) cross-sections that can be used together with the plate geometry in the analysis of the available BSTs. The ASD exhibits the character of acting loads in such a way that designers can adequately select the beam types to accommodate better tension-compression, bending and torsion loads. Consequently, the ASD highlights an influence of the plates (shells) geometry on the load-bearing capabilities of a new design structure. The ASD also contrasts the loads and load cases that have an impact on the structural stiffness of new structures and require improvements in the design. More importantly, the ASD makes all of these benefits possible within one FE model (FEm).

Our work illustrates the ASD for a real use case that proposes a new structure design for an electric-driven L7e vehicle. The ASD provides valuable concepts of a new structure with great potential for

a lightweight design, adequate stiffness and useful suggestions for the structure type best suited to the acting loads. These examples of new eQuad structure proposals demonstrate the universal character of the ASD that can be employed to design new structures in numerous fields of mechanical engineering such as the aerospace, automotive, light and heavy machinery, rail industries.

1.2 Extracting Requirements for the ASD

The mechanical and automotive industries are currently postulating the need for a design method that minimizes the number of vehicle prototypes (or even eliminates prototyping test stages) and delivers robust design verification [19], [24] and [25]. Consequently, these industries also require an approach that permits engineers to build the first concept models with the reduced utilization of computer-aided-design (CAD) tools and apply optimization technologies during the stages of product development so that the development process of a new vehicle becomes completely virtual.

To cope a current systematic approach (which consists of four main phases [26] and [27] such as (1) planning and task clarification, (2) conceptual design, (3) embodiment design, and (4) detail design,) for the design process of a new part or item with simulation technologies, Sellgren [28] postulated a simulation-driven design process (SDDP). The SDDP supports the design process by providing required pieces of information from modeling and simulation techniques. This profitable input allows engineers to reduce work time to acceptable levels and allows for earlier design changes during the development process. The SDDP, however, offers any opportunity to discuss available BSTs.

Engineers search for a design method that allows for innovative and optimal design solutions of available BSTs. Osborne et al. [29] presented the idea for a meth-od of vehicle concept designs. This approach utilizes simple geometrical elements such as beams and plates to describe the rough geometry of a new vehicle structure. In addition, such a rough defined model enables designers to collect engineering data: inertia components, principle force values, rigid body analysis, etc. Although engineers can obtain a rough geometrical description of a new structure, this approach considers no possible way of transition for the geometrical models of bionic shapes. Moreover, this approach demonstrates a lack of optimization technologies that allows for the consideration of a suitable BST.

Compared to Osborne's idea, Steinwall and Viippola [30] demonstrated a design method that combines optimization technology and modern product development. This method applies simulations, optimizations (including TO) and CAD tools to the trial and error design process of a new structure. However, this approach restricts contemporary studies of potential BSTs and different material types within one model with the multiple iterations. Therefore, the changes in the design provoke the actualization of the base line model that adds the extra design iterations. Nevertheless, the transition of bionic shapes into a geometrical model is treated insufficiently, resulting in the difficult enhancement of geometrical models.

Each designer requires that a CAE method transforms bionic TO results into engineering-based models. Baskin el al. [31] proposed a design method that attempts to transform the bionic shapes of TO results into beam-based geometrical models. The beam-based models are further improved to shell-based models with the adaptation of hand-determined beam sections. TO is applied for the generation of load paths. Consequently, other optimization technologies are utilized upon request to optimize one explicitly defined type of the BIW. As a result, the explicitly defined BST prevents simultaneous consideration of the various BSTs in this method. Nonetheless, this approach discloses a lack of examination for different material types such as composites and sandwiches. Moreover, this method provides no opportunity to select, allocate and optimize arbitrary beams together with plate-based geometry.

1.3 Description of the ASD

We propose the ASD method as an extension of our Integrative CAE-driven design process (ICDDP), published earlier in [32]. The ICDDP works as a framework for the ASD and this ICDDP is divided into three essential engineering phases of a new structure design: conceptual design, design crystallization and design sophistication (Fig. 1). Fig. 1 demonstrates the application area of our ASD within the ICDDP. Fig. 1 also depicts the main steps and phases of the ICDDP together with the detailed view of design, modeling and calculation techniques. For each step, there are specified inputs, tasks to perform and defined tools (including optional tools) to apply.

The design sequences of the ICDDP and the ASD employ only one simulation software package (Altair OptiStruct®) that supplies the necessary simulation and optimization methods. It is possible to incorporate other types of software for the ICDDP and ASD if

they are requested. The main steps and design phases of the ICDDP as well as the ASD are universal and to execute them, the other types of software that provide crucial simulation and optimization methods – either partially or all within one software environment – can also be utilized.

As a result of the TO, the bionic shapes of new structures need to be translated into one of the available and selected BSTs. Engineers utilize beams and plates (shells) to represent the fundamental engineering geometry that constitutes all available BIWs. For this reason, our ASD utilizes these fundamental structural elements to deliver new structure concepts. Comparing different types of BIWs, one can assess the qualitative concentration of these fundamental structural elements through available BSTs. Table 1 summarizes the concentration of the available BSTs. This comparison is based on the definitions of the available BSTs **[9]** to **[12]**, visual assessment of qualitative fundamental geometry and its dominant geometrical shapes.

In fact, Table 1 affirms the domination of one fundamental structural element over the others for the specific BST, e.g. beams over plates for an aluminum space frame (ASF). Consequently, we assumed that the investigation of the available BSTs requires simultaneous analysis and optimization for beams and plates within one calculation-simulation model.

To perform such investigation of the available BSTs, the ASD depends upon the layout and its criteria that steer this investigation. Fig. 2 shows that the definition of the available BSTs is influenced by the economic, materials and manufacturing constraints. These three groups of constraints determine the main characteristics of the available BSTs. This observation, for example, can be noticed for the tubular space frame and space frame where the main differences result from the applied materials (steel versus aluminum), production quantity and joining technology (aluminum requires the more sophisticated approach). Despite these fundamental differences, industries also utilize the space frame design for the structures made of steel **[9]** to **[12]**.

Table 1. *Qualitative distribution of the BIW fundamental engineering structural elements*

BIW types	1D – beams	2D – plates	BIW types	1D – beams	2D – plates
TSF	High	Low	SU	Low ÷ med.	High
SSF	High	Low ÷ med.	AU	Med.	High
ASF	High	Low ÷ med.	CM	Low	High
BOF	Med. ÷ high	High	HS	Low ÷ high	Low ÷ high

Where: TSF – tubular space frame; SSF – steel space frame; ASF – aluminum space frame; BOF – body-on-frame; SU – steel unibody; AU – aluminum unibody; CM – composite monocoque; HS – hybrid structure; Med. – medium

Considering the distribution of the fundamental engineering geometry (beams and plates) **[9]** to **[12]**, one can define the prioritizing of such geometrical

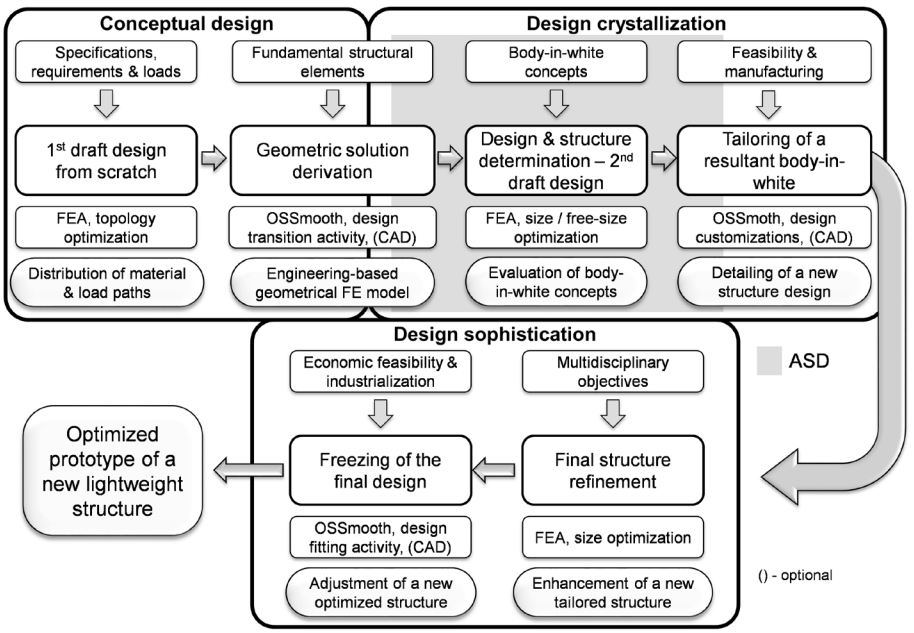

Fig. 1. *ASD as an extension of the ICDD*

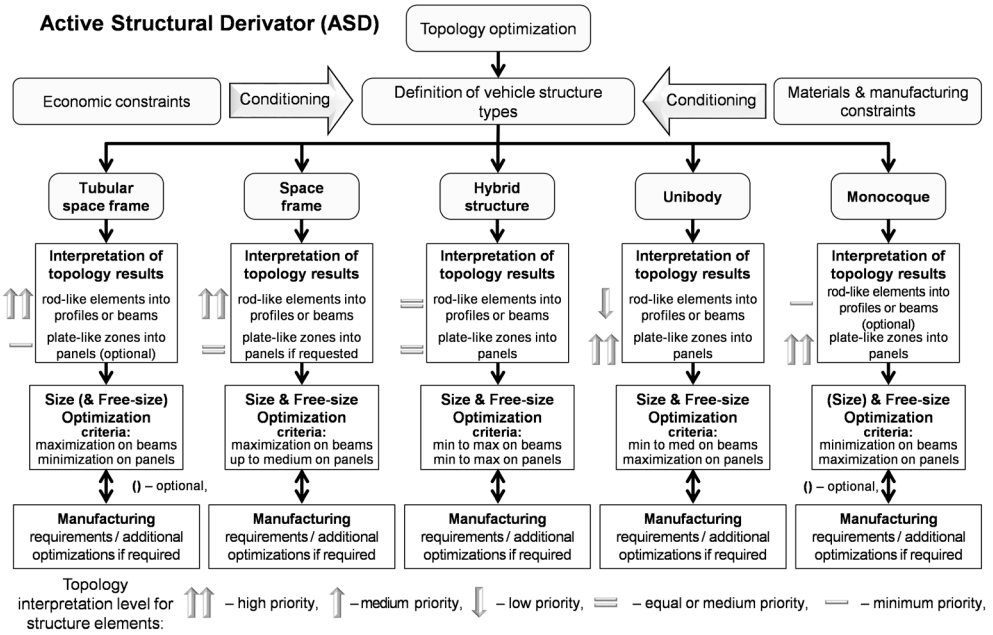

Fig. 2. *Steering criteria for the ASD and the applied optimization techniques*

elements for an FEm obtained from the geometric solution derivation step (Fig. 2). This prioritizing actually constitutes the steering criteria of the ASD by maximizing and / or minimizing the load-bearing intensity for one of the fundamental geometrical elements. Additionally, the ASD provides the opportunity to include special manufacturing requirements that take into account joining technology, testing of lightweight materials (e.g. sandwich composites) as well as extra optimization runs (to reveal more detailed optimization results) if required (Fig. 2).

Table 2. *Steering methodology for the ASD*

BIW structure types	Optimization methods	Prioritizing for 1D elements	Prioritizing for 2D elements
Tub. space frame	SO (/FSO)	Maximization	Minimization
Space frame	SO / FSO	Maximization	Up to medium
Hybrid structure	SO / FSO	Min to max	Min to max
Unibody	SO / FSO	Min to med	Maximization
Monocoque	FSO (/SO)	Minimization	Maximization

Where: BIW – body-in-white; Tub. – tubular; SO, FSO – size and free-size optimization, respectively; (/*) – optimization upon request; Min – minimization; med – medium; max – maximization

The main idea behind the steering methodology is to obtain a BST selected by influencing the load distributions throughout the load-bearing profiles and plates and picking the useful optimization methods or a combination thereof (Fig. 2). Table 2 demonstrates the steering methodology for the ASD. For the reason of simplicity, we chose five different BSTs - tubular space frame, space frame, hybrid structure, unibody and monocoque - to highlight the ASD methodology.

The steering methodology of the ASD utilizes two optimization methods to satisfy the load-bearing capabilities of a new structure by prioritizing the distribution of acting loads throughout the one dimensional (1D) and/or two dimensional (2D) geometrical engineering elements. Thus, the steering methodology sets the limits for the applications of fundamental engineering geometry.

We investigated the ASD by holding this discussion for the real use case of a new eQuad structure. The employment of the ASD raises the following questions regarding the embodiment design phase:

- How can the load-bearing be indicated throughout the arbitrary and defined beams of a new structure to provide knowledge about the tension-compression, bending and torsion loads?
- Is it possible to select, allocate and optimize various beam types together with the plate (shell) geometry for the different BSTs such as tubular space frame, space frame, hybrid structure, unibody and monocoque?
- How can the influence of the plate (shell) geometry be assessed for the load-bearing

capabilities of a new structure that consists of beams and plates?
- How can the bionic TO results be transitioned into manufacturable geometry that exploits the design suggestions of the TO efficiently?
- How should an optimized FEm be prepared to discuss and analyze the different BSTs for a new structure design within one FEm?
- How can the ASD be executed to deliver different proposals for the available BSTs of a new eQuad structure?
- Is it possible to consider the composite and sandwich-composite materials for the ASD of the available body-in-white structure types?
- How can the load cases be revealed that influence mostly the structural stiffness of a new structure and advise about improvements in design concepts?

The next sections provide the answers to the above-listed questions.

2 APPLICATION OF THE ASD

To take full advantage of beam and plate (shell) elements in a new structure, engineers need to know the distribution of the load-bearing throughout all beam elements of a new structure. This section examines the arbitrary and defined beams, their combinations with plate (shell) geometry, a system identification for such combinations, and composite materials for plate geometry with the conjunction of the arbitrary and defined beams. To understand the ASD results of five picked BSTs (Section 2.2) for a new L7e vehicle structure, one needs to test this ASD method on a small scale (Section 2.1) to enlighten the relationship between the beams and plates (shells).

2.1 Beams and Plates as a Fundament to Understand the ASD

2.1.1 ASD - Universal Design Approach for Arbitrary and Defined Beams

We proposed the universal design approach (UDA), which is also one of the ASD design steps, for arbitrary and defined beams that delivers the load-bearing's distribution and allows for the optimization of the selected beam elements. The box beams were selected as a special case of the arbitrary beams to demonstrate the capabilities of the UDA for the defined beam types and because the box cross-sections are characterized, compared to other cross-sections with the constant area, by the highest buckling stiffness, a great section modulus for bending and a significant section modulus for torsion loads [33]. The box cross-section offers flat surfaces that allow for easier packaging and connections of additional accessories and attachments.

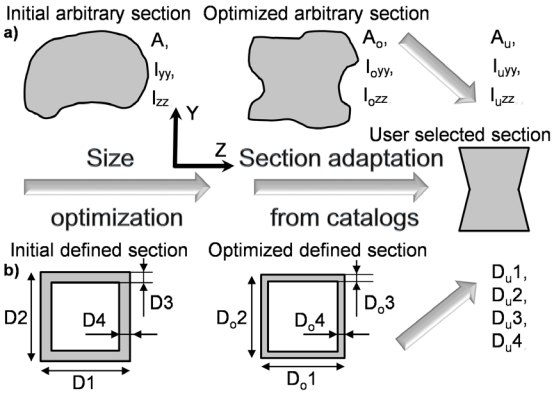

Fig. 3. *ASD – universal design approach for a) arbitrary, and b) defined beams*

Fig. 3 illustrates our UDA methodology for arbitrary (Fig. 3a) and defined (Fig. 3b) beams. A, A_o, A_u, Iyy, Izz, $I_o$yy, $I_o$zz, $I_u$yy, $I_u$zz are the cross-sectional areas and second moments of area for initial, optimized and user-selected arbitrary beam cross-sections, whereas D1, D2, D3, D4, D_o1, D_o2, D_o3, D_o4, D_u1, D_u2, D_u3, D_u4 are the dimensions of the initial, optimized and user-selected for a defined beam cross-section (e.g. box, channel), respectively. The beams of the UDA can be modeled with different isotropic materials such as steel, aluminum and titanium.

The UDA offers two ways to optimize the beam elements and collect essential distribution of beams' load-bearing capabilities. The first general way (Fig. 3a) employs the arbitrary beams that provide the values of the cross-sectional areas and second moments of area (for both principal cross-sectional coordinate axes) after the optimization run. As the cross-sectional parameters are independent for the arbitrary beams, the value of the cross-sectional areas indicates the changes in tension-compression loads and the second moments of cross-sectional area indicates bending and torsional loads. Designers applying the size optimization (SO) [34] and [35] that optimizes the properties (e.g. length, diameter, height, width) of structural elements to provide required solutions obtain the optimized values of the cross-sectional areas and second moments of area. These values of the arbitrary beam cross-sectional parameters serve to select the real beam cross-sections. Consequently, engineers can select the real beam cross-sections that

bear the acting load sufficiently and grant specific requirements given. This selection matches the optimized cross-sections to the real cross-sections from industrial profile catalogs [36] and [37], which can also be new or the preferred one.

The second detailed way (Fig. 3b) makes use of beam elements with the defined cross-sections. As a result of the SO, the user achieves the cross-sectional dimensions that represent a concrete defined beam cross-section (e.g. box, channel). The values of the cross-sectional dimensions for a defined cross-section communicate the distribution of the load-bearing less simply due to the functional relationship between these cross-sectional dimensions. This inconvenience overcomes the possibility of adopting the beam cross-sections directly from industrial profile catalogs [36] and [37], which helps designers deliver new structure concepts more rapidly and efficiently.

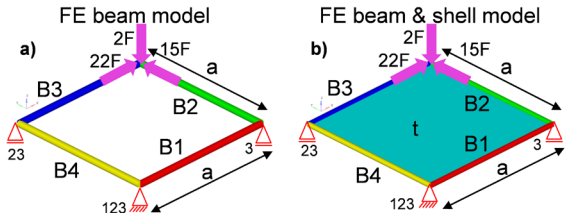

Fig. 4. *ASD – FEms: a) beams, b) beams and shell*

We prepared the FE beam model for the arbitrary and defined box beam cross-sections (Fig. 4a) to test the UDA methodology. The FE beam model (Fig. 3a) consisted of four beam elements (called B1 to B4) with the length a = 100 mm and these four beams were made of steel (Table 3). Three forces that act in three principal axial directions (x, y, z), with the values F = 1 kN multi-plied by corresponding factors such as x = 22, y = 15 and z = 2, were applied to this FEm (Fig. 4). The FEm was constrained to the ground by blocking the relevant degrees of freedom (xyz, yz, and z) in the frame's corners.

The optimization runs were conducted in this work for the constrained values of displacements and the function to minimize was volume or total volume, respectively. The authors of this work tested the UDA for the arbitrary and defined beams by optimizing the FE beam model for the given intervals of the cross-sectional parameters (A is 1.96 mm^2 to 66.0 mm^2; Iyy, Izz 7.8465 mm^4 to 1355.8 mm^4) and dimensions (D1, D2 5 mm to 12.5 mm; D3, D4 0.1 mm to 1.5 mm). The displacements were limited in the point of the force applications to x ≤ 11.0 mm, y ≤ 0.55 mm, and z ≥ -5.95 mm and the values were specially selected to highlight the optimization process.

Table 3. *Material properties for the optimization runs*

Material	ρ [kg/mm^3]	E [GPa]	υ [-]
Steel	7.85e-06	210.0	0.30
Q-I CFRP	1.60e-06	78.0 / 78.0	0.06 / 6.5
Balsa wood	9.7e-08	0.4 / 0.4 / 0.2	0.085
Structural foam	1.05e-07	0.11 / 0.11 / 0.2	0.021
Q-I CFRP – Quasi-isotropic carbon fiber reinforced plastics			

2.1.2 *Conjunction of the Plates (Shells) and UDA for Beams*

In this case, the objective was to assess if and how the additional geometry influences the results of the UDA for beams. The additional objective was to reveal an impact of the plate (shell) geometry on the structure's load-bearing capabilities.

For this purpose, we added the square plate made of steel (Table 3) with dimension a = 100 mm and thickness t = 4 mm to the FE beam model (Fig. 4b). Different isotropic and orthotropic materials can also be applied to model this plate. The plate was optimized together with beams simultaneously by applying free-size optimization (FSO) and SO [34] and [35] to the whole FEm. The FSO optimizes the thickness of each single finite element for the plate (shell) geometry.

Three different cases were examined for the FEm of the beams and plate (Fig. 4b). The first case had the cross-sectional parameters (A is 1.96 mm^2 to 66.0 mm^2; Iyy, Izz 7.8465 mm^4 to 1355.8 mm^4) and dimensions (D1, D2 5 mm to 12.5 mm; and D3, D4 0.1 mm to 1.5 mm). The second case had the smaller intervals of the cross-sectional parameters (A is 1.96 mm^2 to 36.0 mm^2; Iyy, Izz 7.8465÷492.0 mm^4) and dimensions (D1, D2 5 mm to 10 mm; D3, D4 0.1 mm to 1.0 mm) than the first case. The third case differentiated only the allowable resultant displacements of the optimization (x ≤ 2.0 mm, y ≤ 0.55 mm, and z ≥ -5.0 mm) from the first case.

2.1.3 *Conjunction of the Plates (Shells) and the UDA for Beams – System Identification*

The system identification was conducted for the joined FEm consisting of the plate and beams (Fig. 4b). The aim of this investigation was to test if the joined FEm can deliver the system identification that assesses a system for specific sets of system constraints established narrowly.

For this purpose, we explored the system identification for the joined FEm by performing the SO and FSO simultaneously. The joined FEm for the system identification had the cross-sectional parameters (A is 1.96 mm^2 to 66.0 mm^2; Iyy, Izz =

7.8465 mm^4 to 1355.8 mm^4) and dimensions (D1, D2 5 mm to 12.5 mm; D3, D4 0.1 mm to 1.5 mm) but the displacements corresponding to the location of the force applications were more restrictive: $1 \leq x \leq 3$ mm, $0.55 \leq y \leq 0.65$ mm, and $-7.5 \leq z \leq -5$ mm. The plate thickness t was equal to 4 mm.

2.1.4 Conjunction of the plate made of composite material and UDA for beams

To check if the conjunction of the plate and UDA for beams works properly for composite materials, the authors of this work investigated the joined FEm (Fig. 4b) with a plate made of the quasi-isotropic carbon fiber reinforced plastic (CFRP). The quasi-isotropic $[0/45/-45/0]_2$ CFPR laminate was prepared in the HyperLaminate® software from Altair® using the values for the single woven ply of CFRP material (Table 3) [38] and [39]. The thickness t was 4 mm and the cross-sectional parameters (A is 1.96 mm^2 to 66.0 mm^2; Iyy, Izz 7.8465 mm^4 to 1355.8 mm^4) and dimensions (D1, D2 5 mm to 12.5 mm; D3, D4 0.1 mm to 1.5 mm), yet the displacements were limited in the point of the force applications to the values of $x \leq 4$ mm, $y \leq 0.55$ mm, and $z \geq -8$ mm.

2.2 ASD – A New Structure for the eQuad

Our ASD is expected to deliver several possible design proposals for a new vehicle structure. For this reason, the ASD was tested on a large scale for an electrified L7e class vehicle called eQuad. The eQuad (Fig. 5) is a quadricycle vehicle that VIRTUAL VEHICLE Research Center adopted and further developed into the full electric-driven quad [40] and [41].

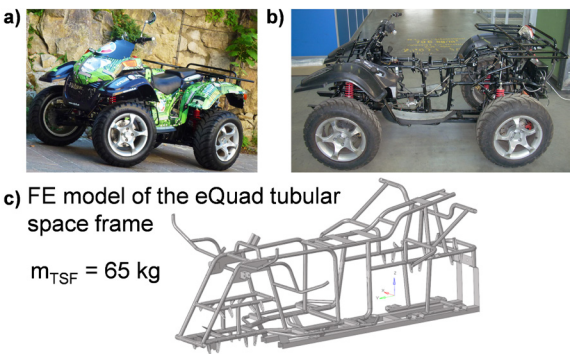

Fig. 5. *Fully electric quadricycle – eQuad: a) complete vehicle, b) tubular space frame, c) FEm of the current vehicle tubular space frame*

The electric power provides the lithium-ion electric batteries to the electric engine. During the adaptation work, the research center converted the original tubular space frame to accommodate the components of the electric powertrain by applying the conversion design approach. The vehicle is capable of reaching 45 km/h and traveling a distance of 30 km. The vehicle is rated for the maximal permissible laden weight of 550 kg including two occupants and luggage; the total mass of the vehicle tubular space frame, which includes the lug-gage rack, brackets for the powertrain and body styling covers, is 82 kg. Fig. 5c displays the FEm of the current eQuad tubular space frame that exemplifies only the fundamental BIW of the eQuad and it weighs 65 kg.

2.2.1 ASD – Geometric solution derivation step for TO results

The ASD requires a geometrical FEm to discuss the various BSTs. The geometrical FEm was obtained by utilizing the geometric solution derivation step of the ICDDP that allows engineers to translate the TO results [32] from the conceptual design phase of the ICDDP.

Fig. 6 exhibits the geometric solution derivation step for the transition of the bionic TO results (Fig. 7a). The transition process starts with the identification of the most visible load paths and material distributions with the densities near 1.0 that form the lines of the force flows (Fig. 7b). Knowing the load paths and material distributions, engineers assess the characteristics of acting loads in the resultant design proposals by identifying shear fields and tension-compression areas [32].

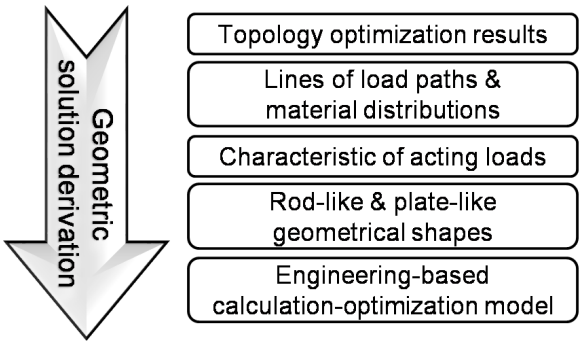

Fig. 6. *Geometric solution derivation step for the transition of the bionic TO results*

Additionally, the lines of the load paths and material distributions help to recognize the rod-like and plate-like geo-metrical shapes from the bionic TO results. This recognition results in the geometrical transition of the bionic TO results into an engineering-

based calculation-optimization model that consists of beam-like and plate-like geometrical engineering elements (Fig. 7c). The geometric solution derivation step can be performed in any aided engineering software that contains basic functions of 3D modeling.

2.2.2 ASD – 1D-2D FEm

The geometric solution derivation step delivered the calculation-optimization FEm (Fig. 7c) of a new structure to the ASD. Fig. 7c presents the 1D-2D FEm of a new structure design for the eQuad. The 1D-2D FE model for the ASD consisted of the beam (1D) and shell (2D) elements. The beam elements of this 1D-2D FEm allowed for the different cross-sections: defined and arbitrary. The material model MAT1 was selected to describe the linear, temperature-independent, isotropic material properties of the FEm geometry that is made of steel (Table 3).

The steel material was chosen due to its higher strength to density ratio and better stiffness to weight ratio than aluminum and magnesium (i.e. in the case of high-strength steels) [42]. These steels can also be paired with other materials to deliver modern hybrid and innovative multi-material designs [43]. The economic ad-vantages of the manufacturing process favor steels [44] over other materials. More importantly, the steel simplifies the simulation-optimization process compared to the composites, while at the same time offering similar stiffness, allowing for the generalization described in the previous work [32].

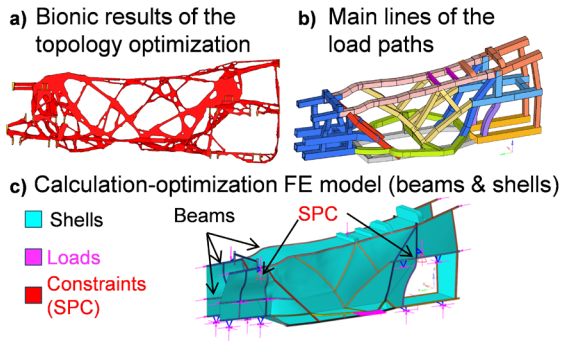

Fig. 7. *Preparation of the 1D-2D FE model for the ASD*

The same loads were applied as they were prepared for the conceptual design phase of a new structure [32]. These loads consider different load scenarios such as static, driving and crash situations that result in 19 different load cases. The prepared load cases define the forces for: vertical bending, front and rear torsion, front and rear braking, cornering, front and rear vertical bumps, bending for front and rear axles, and equivalent static front, rear and side crashes.

The values of these defined forces were obtained by applying a first-order model approach [45] that allows for analyses of what-if questions during the early design phase. We established the additional equations for the models of the first-order approach that calculate the forces for the short-long-arm suspension type under driving conditions. The calculated forces of driving conditions took into account the dynamic behavior with the additional coefficients [45]. The forces obtained were put onto the attached points of the vehicle suspension. A work-energy balance approach [45] was utilized to determine the acting forces for the equivalent static crash load cases. Furthermore, the forces for the bending and torsion load cases were determined by executing the FE analyses for the original structure of the eQuad [46]. We executed the FE simulations for the complete FE eQuad model with the original space frame to assess the vehicle behavior during accidents [46].

The 1D-2D FEm (Fig. 7c) employed the inertia relief approach [34] and [35] to enhance optimization convergence and simulation stability in the case of unconstrained structures. The optimization runs of the all ASD cases minimized the total volume function while the optimization constraints set the optimization domain, limiting the maximal displacements corresponding to the forces from the defined load cases.

We estimated the values of these displacements by conducting the additional FE linear simulations and extracting the displacements from the realized finite element analyses (FEA) [46]. In the case of the crash loads, the displacements were adjusted by allowing larger de-formations so that the other loads could influence the optimization results more evidently.

42 different beams and 22 shell components were specified to define the geometry of the 1D-2D FEm for a new eQuad structure. This frame-shell FEm contained 80 optimization constraints on the resultant displacements; the design variables were 126 (127 for FEm with shells) for the beams with the arbitrary cross-sections and 168 (169 for FEm with shells) for the beams with the defined box cross-sections.

2.2.3 ASD – The Tubular Space Frame

A vehicle tubular space frame is the structure that consists of joined together (mostly welded) tubes or pro-files, different in size and dimensions. The

presence of plate (shell)-like geometry is limited to a minimum and accommodates the packaging purposes.

For this reason, the shell geometry was excluded from the 1D-2D FEm, thus allowing for maximal prioritizing of 1D elements. The cross-sectional parameters and dimensions varied for the arbitrary beams: A 0.44 mm^2 to 896 mm^2, Iyy, Izz = 0.0895 mm^4 to 470,700 mm^4 and the box beams: D1, D2 1.2 mm to 60 mm, D3, D4 0.1 mm to 4 mm.

2.2.4 *ASD – The Space Frame*

A vehicle space frame is the advanced BST that is based on the profile-like (beams) geometry in the structure layout. The shell-like geometry supports the beams in their load-bearing capabilities. The acting loads are mainly distributed among the beams, whereas the shells reinforce the structure in the case of the shear loads.

We prepared the 1D-2D FEm that contains the beam and shell geometry (Fig. 7c). The cross-sectional parameters and dimensions varied for the arbitrary beams: A 0.44 mm^2 to 896 mm^2, Iyy, Izz 0.0895 mm^4 to 470,700 mm^4 and the box beams: D1, D2 1.2 mm to 60 mm, D3, D4 0.1 mm to 4 mm to prioritize the beam-like geometry. The thickness of the shell geometry changed between 0.0 and 1.0 mm.

2.2.5 *ASD – The Hybrid Structure*

A hybrid structure for vehicles is defined as a mix of engineering geometry types, in which the domination of profiles or shells depends on the designer's ideas.

The entire 1D-2D FEm (Fig. 7c) was utilized with the two different intervals of cross-sectional parameters and dimensions. The first setup of the design variables was set for the arbitrary beams: A 0.44 mm^2 to 144 mm^2, Iyy, Izz 0.0895 mm^4 to 7872 mm^4 and box beams: D1, D2 1.2 mm to 20 mm, D3, D4 0.1 mm to 2.0 mm. The second setup was set for the arbitrary beams: A 0.44 mm^2 to 896 mm^2, Iyy, Izz 0.0895 mm^4 to 470,700 mm^4 and box beams: D1, D2 1.2 mm to 60 mm, D3, D4 0.1 mm to 4 mm. The thickness of the shells varied from 0 mm to 0.95 mm for the first setup and 0 to 0.5 mm for the second setup.

2.2.6 *ASD – The Unibody*

A vehicle unibody is the modern BST that utilizes the combination of shells and profiles and the shell geometry dominates in the structural design. The shell geometry also enhances the load-bearing capabilities for shear loads. The profiles are used for very specific load-bearing structural elements, e.g. the B-pillar.

We utilized the entire 1D-2D FEm to achieve the unibody structure design. The cross-sectional parameters and dimensions changed for the arbitrary beams: A 0.44 mm^2 to 144 mm^2, Iyy, Izz 0.0895 mm^4 to 7872 mm^4 and box beams: D1, D2 1.2 mm to 20 mm, D3, D4 0.1 mm to 2 mm to prioritize the beam-like geometry. The thickness of the shell geometry varied between 0 and 0.85 mm.

2.2.7 *ASD – The Monocoque*

A monocoque structure for vehicles is the special case of the unibody BST and is characterized by employing the shell-like geometry for the whole structure design. The number of the profiles is reduced to minimal applications for the specific parts of a new structure (e.g. the A-pillar).

All profiles in the 1D-2D FE (Fig. 7c) model were blocked by modeling them as the box cross-sections with small dimensions (the arbitrary beams: A = 3 mm^2 to 59.04 mm^2, Iyy, Izz 1.25 mm^4 to 693.5232 mm^4 and the box beams: D1, D2 2 mm to 10 mm, D3, D4 0.5 mm to 1.8 mm; the higher values were used for the elements under crash forces) and therefore only permitted optimization for the shells. The thickness of the shell geometry changed be-tween 0 and 6 mm.

3 APPLICATION OF THE ASD - RESULTS AND DISCUSSION

3.1 Beams and Plates as a Fundament to Understand the ASD

The FE calculation results reported in this section correspond with the method testing on a small scale de-scribed in Section 2.1. These results are provided with additional comments. The ASD results for the arbitrary beams reveal the cross-sectional parameters that lead to a proper selection of the suitable beam section, whereas the box beams indicate the possible design proposals based on the industrial types of the beam cross-sections. The figure legends were purposely left inconsistent to reveal more valuable data and the total mass describes the sum of all the components' mass.

3.1.1 *ASD - UDA for Arbitrary and Defined Beams*

The aim of this investigation was to highlight the benefit of the UDA (as a part of the ASD) for the arbitrary and defined box beams. We conducted two

optimization runs for the same FEm (Fig. 4a) for both the arbitrary and defined box cross-sections.

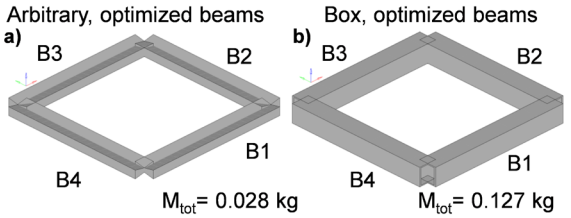

Fig. 8. *ASD results for the beam cross-sections: a) arbitrary, b) box*

The SO results presented in Fig. 8a demonstrate the values of second moments of area for the arbitrary beams. The values of the area are missing in Fig. 8a due to the mathematical description of the arbitrary beam cross-section where the area is only a parameter. The possible shape of the area would introduce the functional relationships (additional constraints) between the area and basic dimensions of the cross-section, which leads to the defined beams. The areas of the arbitrary beams indirectly represent the total resultant mass in Fig. 8a. The optimization run sets the cross-sectional parameters for the arbitrary beams to minimal possible values that minimize the weight and accommodate the acting loads.

The second moments of area for the arbitrary case illustrate this observation more precisely because of the variables of this beam cross-section type that are optimized independently due to the theory of arbitrary beams **[34]** and **[35]**. The values of the $I_o zz$ were set to a high level to increase the bending stiffness of the arbitrary beams (Fig. 8, Table 4). The area of the B2 beam also increases to bear the compression load.

Table 4. *Summary of the UDA for the arbitrary and box beams*

Fig. 8		B1	B2	B3	B4
Arbitrary	A_o [mm²]	7.85	12.82	7.30	7.34
	$I_o yy$ [mm⁴]	211.05	211.06	211.05	211.06
	$I_o zz$ [mm⁴]	1335.80	1335.80	1335.80	1335.80
Box	$D_o 1$ [mm]	12.50	12.50	12.50	12.50
	$D_o 2$ [mm]	12.50	12.50	12.50	12.50
	$D_o 3$ [mm]	1.08	1.06	1.05	1.06
	$D_o 4$ [mm]	0.68	0.67	0.66	0.67
Resultant displacements [mm]: arbitrary x = 11; y = 0.55; z = -5.46; box x = 11; y = 0.18; z = -5.84					
Compliance [kNmm]: arbitrary 130.701; box 128.211					

In the case of the defined box beams, the optimization results in the maximal external dimensions of the box cross-sections that react to the bending and compression loads (Fig. 8, Table 4). The case of the arbitrary beams displays a slightly higher total compliance (the inverse of stiffness) **[34]** and **[35]** than that of the defined box beams (Table 4). This finding means that the defined box beams exemplify a stiffer design. The arbitrary beams show much lower total mass compared to the defined box beams because the arbitrary beams evidence the total resultant mass the uncoupled cross-sectional parameters that satisfy the given boundary conditions theoretically.

Consulting the available catalog of industrial beam products **[36]** and **[37]**, the authors of this work propose the beam with the box cross-section of 13 mm × 13 mm × 1.6 mm to satisfy the design suggestions from the UDA for defined beams. For the arbitrary beams, two solutions can be found: the same as the previous box section and the rectangular box section of 15 mm × 10 mm ×1.5 mm. The last beam type can be applied if there is no geometrical limitation to the design space. These facts affirm that the UDA works for the arbitrary and defined beams and allows for various and broad adaptations of different beam cross-sections.

3.1.2 Conjunction of the Plates (Shells) and UDA for Beams

We tested the conjunction of the plate (shell) geometry and the UDA for beams to highlight the benefits of such a combination. Fig. 9 presents the SO and FSO results for three different optimizations, such as the addition of plate (shell) geometry to the FEm of the beams (the first case, Figs. 9a and b), design space restriction (the second case, Figs. 9c and d) and tougher limits on the displacements (the third case, Figs. 9e and f) and two different types of the beam section: arbitrary and box.

The addition of the extra plate (shell) geometry results in the lower values of the areas and second moments of area for the arbitrary beams (Table 5, Fig. 9a). The resultant values of the first case (Table 5) indicate the load-bearing characteristics such as bending and tension-compression that result from the acting loads. To improve the structural stiffness, the arbitrary beams utilize the thickness of the plate in the corners. For the second case of the design space restriction (Table 5, Fig. 9c), the SO and FSO results for the arbitrary beams are the same as for the first case because this solution satisfies both analyzed cases.

In the case of the restrictive displacement limits, the optimization sets the second moments of area higher than the previous values of the first and second cases. The values of the second moments of area for the arbitrary beams affirm the presence of the bending loads (Table 5). The cross-sectional areas of the arbitrary beams remain on the same level as in the first and second cases

(Table 5). The optimization employs the plate thickness to fulfill the optimization constraints. These employed parts of the plate (Fig. 9e) form the diagonal shape and gain the plate thickness in the corners of the plate.

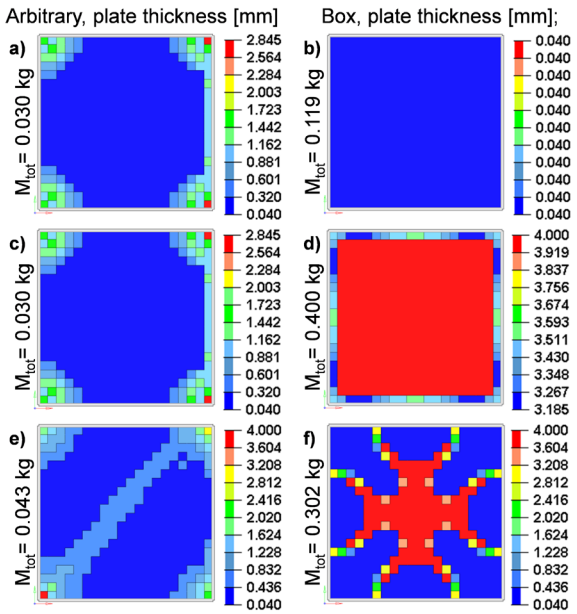

Fig. 9. *ASD results of the frame-plate FEms: a, b) plate addition to the FE beam model, c, d) design space restriction, e, f) restrictive displacement limits*

Owing to the thickness employment, the optimized frame-plate model of the arbitrary beams weighs 0.043 kg, more than the optimized frame-plate model (0.030 kg) for the first and second cases. Considering the total resultant compliance (Table 5) for three cases of the arbitrary beams, the optimized frame-plate model (29.624 kNmm) from the third case displays the stiffest design.

The simultaneous SO and FSO optimizations of the frame-plate model consisting of the box beams demonstrate slightly different results. The optimization of the frame-plate model with the added plate geometry and the box beams reports almost the same values of the cross-sectional dimensions for the first case (Table 5) as those of the pure frame model (Table 4). This remark can also be noticed in Fig. 9b where the optimization neglects the plate thickness. Compared to the first case, the second case of the design space restriction for the box beams reveals the more contrasting results. The optimization places the cross-sectional dimensions to fulfill the optimization boundaries and minimize the weight (Table 5). Due to the insufficient stiffness of the box beams, the optimization makes use of the whole plate to assure the requested stiffness (Fig. 10d). In the third

Table 5. *Conjunction of the plate (shell) and UDA for beams – summary*

Figs. 9a, b / 1st case		B1	B2	B3	B4
Arbitrary	A_o [mm²]	2.01	7.57	2.01	2.1
	I_oyy [mm⁴]	212.89	212.89	212.89	212.89
	I_ozz [mm⁴]	7.85	7.85	7.85	7.85
Box	D_o1 [mm]	12.5	12.5	12.5	12.5
	D_o2 [mm]	12.5	12.5	12.5	12.5
	D_o3 [mm]	0.77	0.77	0.77	0.77
	D_o4 [mm]	0.81	0.81	0.81	0.81
Resultant displacements [mm]: arbitrary x = 7.35, y = 0.55, z = -5.95; box x = 4.52, y = 0.19					
Compliance [kNmm]: arbitrary 90.918; box 57.100					
Figs. 9c, d / 2nd case		B1	B2	B3	B4
Arbitrary	A_o [mm²]	2.01	7.57	2.01	2.1
	I_oyy [mm⁴]	212.89	212.89	212.89	212.89
	I_ozz [mm⁴]	7.85	7.85	7.85	7.85
Box	D_o1 [mm]	10	10	10	10
	D_o2 [mm]	10	10	10	10
	D_o3 [mm]	0. 82	0. 82	0. 82	0. 82
	D_o4 [mm]	0. 83	0. 83	0. 83	0. 83
Resultant displacements [mm]: arbitrary x = 7.35, y = 0.55, z = -5.95; box x = 0.27, y = 0.10, z = -5.93					
Compliance [kNmm]: arbitrary 90.918; box 9.673					
Figs. 9e, f / 3rd case		B1	B2	B3	B4
Arbitrary	A_o [mm²]	2.59	7.92	2.57	2.34
	I_oyy [mm⁴]	576.50	576.50	576.50	576.50
	I_ozz [mm⁴]	10.36	10.36	10.36	10.36
Box	D_o1 [mm]	12.5	12.5	12.5	12.5
	D_o2 [mm]	12.5	12.5	12.5	12.5
	D_o3 [mm]	1.5	1.5	1.5	1.5
	D_o4 [mm]	1.5	1.5	1.5	1.5
Resultant displacements [mm]: arbitrary x = 2.00; y = 0.55; z = -3.50; box x = 0.77, y = 0.10, z = -3.50					
Compliance [kNmm]: arbitrary 29.624; box 12.757					

case of the tougher limits on the displacements, the optimization puts the cross-sectional dimensions to maxi-mal values to satisfy the boundary conditions. To enhance the frame-plate stiffness, the SO and FSO utilize the plate thickness by forming the central cross-like member (Table 5, Fig. 9f).

Observing the total mass of these three box cases, the first case of the frame-plate model possesses the lowest weight, yet the second case represents the stiffest structure (minimal compliance, Table 5). The observations presented affirm that the conjunction of the plate (shell) and the ADA for beams can deliver new helpful pieces of information to the design process. This conjunction points out not only where the plate (shell) can be improved to withstand the

shear loads by adding extra strips of the geometry, but also exhibits the load-bearing characteristics that engineers identify as compression-tension, bending or torsion fields. The delivering of additional design suggestions constitutes the ASD as the functional methodology.

3.1.3 *Conjunction of the Plates (Shells) and the UDA for Beams – System Identification*

The system identification run was performed for the conjunction of the plate (shell) and the UDA for two beam cross-sections: arbitrary and defined box beams. The aim of this system identification was to examine if the FEm (Fig. 4b) can additionally provide the solutions under the highly restricted sets of the model constraints. Fig. 10 and Table 6 display the ASD results of the system identification for the arbitrary a) and box b) beams.

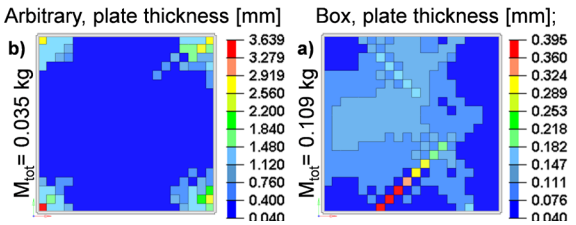

Fig. 10. *ASD results of the system identification for the frame-plate FEms: a) arbitrary beams, b) box beams*

Table 6. *System identification for the frame-plate FEms – summary*

Fig. 10		B1	B2	B3	B4
Arbitrary	A_o [mm^2]	1.99	7.02	1.99	1.99
	$I_o yy$ [mm^4]	146.23	146.23	146.23	146.23
	$I_o zz$ [mm^4]	10.23	10.23	10.23	10.23
Box	$D_o 1$ [mm]	12.5	12.5	12.5	12.5
	$D_o 2$ [mm]	12.5	12.5	12.5	12.5
	$D_o 3$ [mm]	0.79	0.21	0.79	0.92
	$D_o 4$ [mm]	0.83	0.25	0.83	0.95
Resultant displacements [mm]: arbitrary x = 3.00, y = 0.65, z = -7.50; box x = 2.99, y = 0.55, z = -7.50					
Compliance [kNmm]: arbitrary 45.367; box 44.559					

The simultaneous SO and FSO of the arbitrary beams set the second moments of area to bear the bending loads and the cross-sectional beam areas to handle the compression-tension loads as well as minimize the weight (Table 6). To improve the stiffness of the frame-plate model consisting of arbitrary beams, the optimization increases the plate thickness in the plate's corners (Fig. 10a). In the case of the defined box beams, the SO and FSO assign the cross-sectional dimensions to with-stand the bending (torsion) loads and reduce the overall resultant mass (Table 6). These optimizations adjust the structural stiffness of the frame-plate model by utilizing the plate thickness that forms the central reinforcement (Fig. 10b).

Despite the difference in the weights of the arbitrary and box beams, both optimized frame-plate models depict the same stiffness (similar level of the resultant compliance, Table 6). These remarks suggest that the arbitrary beams offer the indications of possible solutions for a given set of requirements, but the box beams present the real one with the more easily applicable cross-sections.

3.1.4 *Conjunction of the Plate Made of Composite Material and UDA for Beams*

The application of CFRP materials was investigated for the plate (shell) within the frame-plate FEm (Fig. 4b). Fig 11 and Table 7 illustrate this application for the plates of the arbitrary a) and box b) beams.

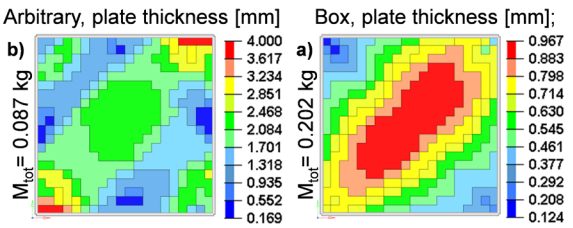

Fig. 11. *ASD results of the CFRP material application for the plate in the frame-plate FEms: a) arbitrary beams, b) box beams*

The simultaneous SO and FSO of the arbitrary beams regulate the values of the second moments of area to bear the bending loads (Table 7). These optimizations also place the cross-sectional areas of the arbitrary beams to limit the overall weight. Since the optimization boundaries were further restrained (Tables 5 and 7) for this application of the CFRP materials (compared to the other cases), the CFRP plate of the arbitrary beams forms the diagonal with the local reinforcements similar (Fig. 11a) to the geometry observed in the steel plate (Fig. 9e) that strengthens the beam-plate structure. For the frame-CFPR plate model of the box beams, the SO and FSO set the cross-sectional dimensions to accommodate the bending loads and moderate the structural weight (Table 7).

To improve the structural stiffness of the frame-CFRP plate, the SO and FSO employ the CFRP plate thickness that creates the diagonal with the center part of the high thickness (Fig. 11b). After optimization,

the defined box frame-CFRP plate model weighs nearly 0.202 kg, which is 0.1 kg less than the frame-plate made of steel. In the case of the arbitrary frame-CFRP plate model, the optimized structure weighs 0.087 kg, which is approximately three times more than the frame-plate made of steel.

Table 7. *CFRP material application for the plate in the frame-plate FEm – summary*

Fig. 11		B1	B2	B3	B4
Arbitrary	A_o [mm²]	14.62	27.19	15.53	16.81
	I_oyy [mm⁴]	305.83	305.83	305.83	305.83
	I_ozz [mm⁴]	7.85	7.85	7.85	7.85
Box	D_o1 [mm]	12.5	12.5	12.5	12.5
	D_o2 [mm]	12.5	12.5	12.5	12.5
	D_o3 [mm]	1.34	1.37	1.33	1.33
	D_o4 [mm]	1.38	1.41	1.37	1.37
Resultant displacements [mm]: arbitrary x = 1.00, y = 0.23, z = -4.00; box x = 1.00; y = 0.11, z = -4.0					
Compliance [kNmm]: arbitrary 16.690; box 15.803					

Considering the total resultant compliance, both the arbitrary and box frame-CFRP plates disclose almost the same structural stiffness (Table 7) and exceed the structural stiffness of the corresponding frame-plate made of steel (Tables 5 and 6). This investigation proves that other material types such as composite materials, CFRPs and sandwich composites (also metal sandwich composites) can be analyzed and optimized by the ASD as well as provide profitable suggestions for a new structure design.

3.2 ASD – A New Structure for the eQuad

The FE calculation results reported in this section match with the method testing on a large scale described in Section 2.2. The ASD results are provided with additional comments. For the reason of available space, we only report the graphical illustrations for the selected and defined (Section 3.2) BSTs. The lists of the resulting values from the optimization runs, which contain 80 optimization constraints and 128 (arbitrary beams) as well as 169 (defined box beams) design variables for each BST, could extend the length of this work excessively.

The ASD results for the arbitrary beams display the cross-sectional parameters and indicate the beams with the load-bearing characteristics that help to select proper suitable beam sections, whereas the box beams reveal the possible design proposals based on the available industrial types of the beam cross-sections. The figure legends were purposely left inconsistent to reveal more valuable data. The total mass presented in the figures describes the sum of all the components' mass.

3.2.1 ASD – The Tubular Space Frame

We obtained the tubular space frame design for a new eQuad structure by performing SO. Fig. 12 presents the geometrical representation of the SO results for arbitrary a) and box b) beam cross-sections.

The SO results of the arbitrary beams (Fig. 12a) graphically display the values of the second moment of area without the values of the cross-sectional areas due to the theory of the arbitrary beams (Section 4.1) **[34]** and **[35]**. The cross-sectional beam areas are indicated indirectly by the total resultant mass (7.44 kg) of a new structure. These SO results of the arbitrary beams deliver the optimal values of the cross-sectional parameters that allow engineers to select the most suitable beam cross-section for the load-bearing. Following the principal ideas of the UDA for beams (information about load-bearing), Fig. 12a indicates the beams where the bending and/or torsion loads dominate. The beams with the dominating tension-compression loads can be identified by analyzing the resultant values of the cross-sectional areas for all arbitrary beams.

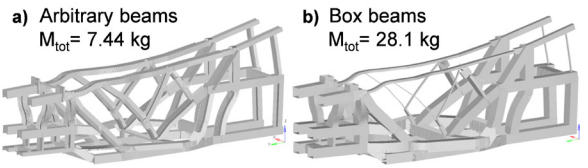

Fig. 12. *ASD results for the tubular space frame design: a) arbitrary beam, b) box beams*

Fig. 12b illustrates the SO results of the optimized cross-sectional dimensions for the box beams. The SO adapted the cross-sectional dimensions to accommodate the acting load. Similar to the arbitrary beams, the values of the box cross-sectional dimensions (Fig. 12b) also suggest the load-bearing characteristics (tension-compression, bending and torsion) by tailoring the proper dimensions of the box cross-sections. In Fig. 12b, there are the beams with the small cross-sections (central upper part of a new structure) as well as with the large cross-sections (central and lower, front and rear parts of the new structure). The new structure consisting of the box beams weighs 28.1 kg because the cross-sectional dimensions of the box beams are related in the functional relationship.

In spite of the difference in weight, the arbitrary and box beams deliver the valuable proposals of a new structure that offer the stiff and lightweight design com-pared to the current structure design (Fig. 5c). The slightly lower compliance for the arbitrary beams (1171.3 kNmm) discloses this solution being stiffer than the box beams (1271 kNmm). These observations suggest that the ASD provides profitable proposals for the tubular space frame design.

3.2.2 ASD – The Space Frame

The space frame design of the new eQuad structure was obtained by utilizing the SO and FSO simultaneously. Fig 13 reports the SO and FSO results of a new structure design for the a) arbitrary and b) defined box beams.

The application of the shells in the 1D-2D FEm of the arbitrary beams influences the values of the cross-sectional areas and second moments of area (Figs. 13a, b). The cross-sectional areas decrease and the second moments of area adapt locally by sizing the correspond-ing values of cross-sectional parameters forcing the shells to bear more loads, especially shear loads. These sized values of the second moments of area indicate the load-bearing characteristics of bending loads. As a result of the great shear load-bearing characteristics, the arbitrary beams with the shells weigh 34.1 kg, which is considerably more than the 7.44 kg of the tubular space frame.

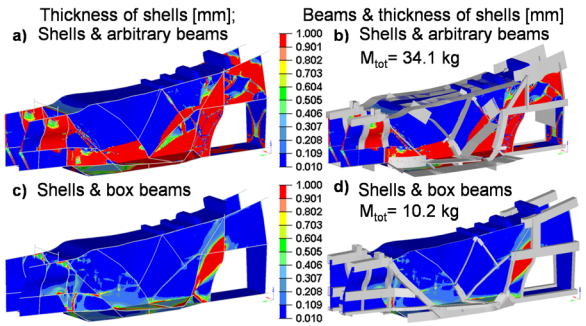

Fig. 13. *ASD results for the space frame design: a, b) arbitrary beams, c, d) box beams*

The shells impact the defined box beams more evidently (Fig. 13b), reducing the total resultant mass to 10.2 kg, which is two times lower than the weight of the tubular space frame (28.1 kg) consisting of box beams. This lower weight results from the combined SO and FSO that set the cross-sectional dimensions of the box beams to minimize the weight and maximize the second moments of area. The reduced cross-sectional areas need a sup-port of the shells to bear the acting loads.

Regardless of the difference between the two resultant weights, the ASD provides the space frame designs with a similar level of compliance: 1762 kNmm for the arbitrary and 1855 kNmm for the box beams. These observations confirm that the ASD can deliver suitable proposals for a new space frame design.

3.2.3 ASD – The Hybrid Structure

We achieved the hybrid structure design of a new eQuad structure by performing the SO and FSO simultaneously for the two setups of the 1D-2D FEm that consists of the arbitrary and defined box beams. Fig. 14 presents the obtained proposals for the hybrid structure designs for the first setup of the arbitrary (Figs. 14a and b) and box (Figs. 14c and d) beams.

Compared to the results of the tubular space frame and the space frame for the arbitrary beams, the shells from the hybrid structure affect the arbitrary beams more evidently. Because of the tighter design space (lower allowable values of the cross-sectional parameters), the SO and FSO minimize the weight of a new structure by setting the suitable values of the second moment of area and reducing the cross-sectional areas of the arbitrary beams.

The simultaneous SO and FSO utilize the shells to improve the load-bearing characteristics of the arbitrary beams. This improvement results in the employment of the large shell surfaces that display the great variety of the shell thickness (Figs. 14a and b). More importantly, the hybrid structure of the shells and arbitrary beams weighs 18.5 kg, which places the hybrid structure in the middle between the proposal designs of the tubular space frame and space frame.

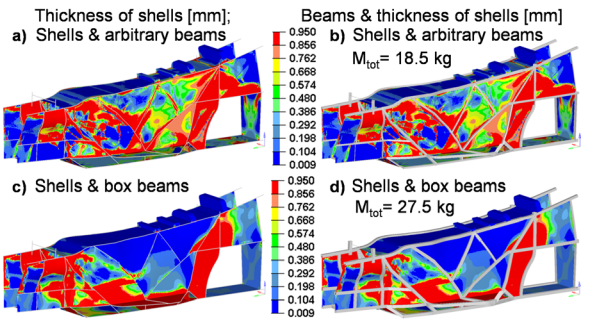

Fig. 14. *ASD results for the hybrid structure design: a, b) arbitrary beams, c, d) box beams*

Similar to the arbitrary beam case, the shells impact the results of the hybrid structure for the box

beams (Figs. 14c and d). The simultaneous SO and FSO adjust the cross-sectional dimensions of the box beams to minimize the weight and bear the acting loads. Because of the tighter design space, the cross-sectional dimensions exhibit maximal values for the external dimensions and moderate values for the internal ones (Fig. 14d).

The optimization uses parts of the shell surfaces to satisfy the given boundary conditions. Owing to the functional relationship of the cross-sectional dimensions, the hybrid structure consisting of the shells and box beams weighs 27.5 kg, which is slightly less than the tubular space frame and considerably more than the space frame.

The less common observations can also be made for the second setup (Fig. 15) of the 1D-2D FEm. The wider design space allows the cross-sectional parameters of the arbitrary beams (Figs. 15a, b) to set the higher values of the areas and second moments of area. The values of the second moments of area, which are presented in Fig. 15b, show the obtained values that indicate the actual characteristics of the acting loads such as bending and (or) torsion.

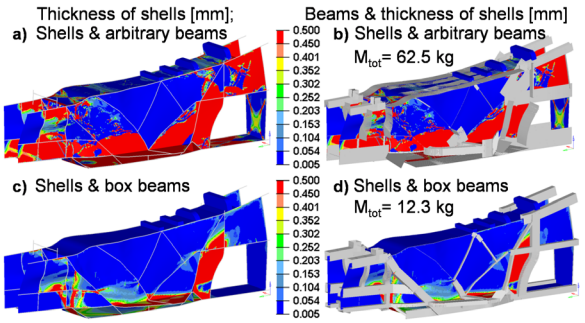

Fig. 15. *ASD results for the hybrid structure design: a, b) arbitrary beams, c, d) box beams*

Compared with the first setup of the hybrid structure and other BSTs, the thick shells dominate more evidently in the new structure, especially in the lower center part. Thus, this hybrid structure weighs 62.5 kg, which reaches the mass of the present eQuad tubular space frame.

In the case of the box beams, the simultaneous SO and FSO assign the external cross-sectional dimensions to the high values and the internal dimensions to the lower ones to minimize the weight (Figs. 15c and d). To enhance the structural stiffness, the optimization exploits the shell surfaces locally. This hybrid structure comprising the box beams weighs only 12.3 kg and bears a re-semblance to the space frame design (Figs. 13c and d).

Considering the level of the total resultant compliances (invert stiffness), the second setup for the arbitrary beams provides more stiffness (2680 kNmm) than the first one (3547 kNmm), whereas the hybrid structure with the box beams from the first setup delivers the toughest design (1531 kNmm vs. 1761 kNmm of the second setup) among all cases of the hybrid structure. The results presented indicate that the ASD produces valuable proposals for the hybrid structure design.

3.2.4 ASD – The Unibody

We obtained the unibody design of the new eQuad structure by simultaneously executing the SO and FSO for the given design space. Fig. 16 reveals the design proposals for the unibody for the arbitrary (a,b) and box (c,d) beams.

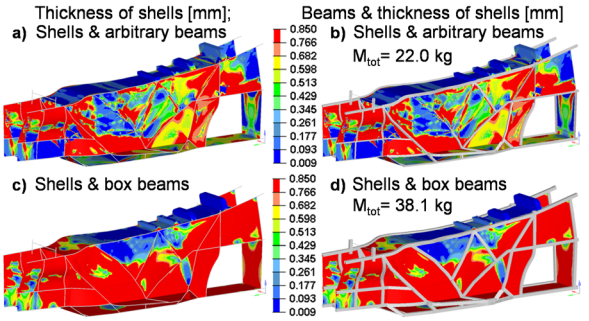

Fig. 16. *ASD results for the unibody design: a,b) arbitrary beams, c, d) box beams*

In the case of the arbitrary beams (Figs. 16a and b), the optimization adjusts the values of the second moments of area between the lower and medium levels. These optimized values disclose the load-bearing characteristics (bending and/or torsion loads) of the arbitrary beams. The SO and FSO position the values of the cross-sectional areas to reduce the total resultant mass. To fulfill the displacement constraints, the optimization utilizes the various thicknesses of the shell surfaces (Figs. 16a and b).

As a consequence of this (SO and FSO) optimization, the unibody design of the arbitrary beams weighs 22 kg. Compared to the presented results of the arbitrary beams for the tubular space frame, space frame and hybrid structure, the unibody consisting of the shells and arbitrary beams displays the medium weight.

The application of the shell geometry in the box beams (Figs. 16c and d) reveals results that show a resemblance to the arbitrary beam case. The

simultaneous SO and FSO optimization assigns high values for the external cross-sectional dimensions and moderate to high values for the internal dimensions to increase the bending and/or torsional stiffness and decrease the overall structure weight. To raise the structural stiffness, the optimization employs shell surfaces with the full thickness (Figs. 16c and d). Consequently, this combined frame-shell weighs 38.1 kg. Considering the total resultant mass of the tubular space frame, space frame and hybrid structure, this unibody design containing the shells and box beams demonstrates a heavier design than the other proposals.

Despite its heavier weight, the unibody design of box beams contrasts the very stiff design; the compliance (1342 kNmm) is relatively low compared to the tubular space frame case. The unibody design of the arbitrary beams demonstrates, however, similar stiffness (3880 kNmm) to the first setup for the hybrid structure. Regarding the observations revealed, the ASD generates profitable design suggestions for the unibody structure.

3.2.5 *ASD – The Monocoque*

The monocoque design was obtained by carrying out FSO for the 1D-2D FEm (Fig. 7c). Fig. 17 presents the design proposals for the monocoque BST for the arbitrary (a, b) and (c, d) box beams.

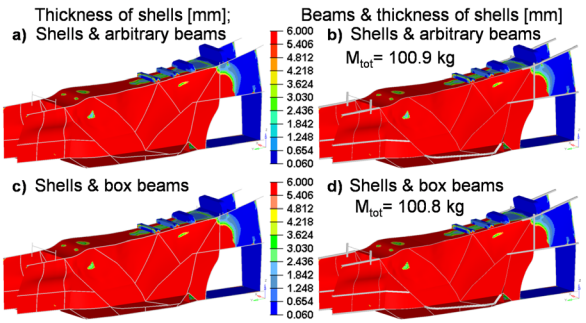

Fig. 17. *ASD results for the monocoque design: a, b) arbitrary beams, c, d) box beams*

Because FSO neglects the optimization of the arbitrary and box beams, the optimization results point out the same thickness distributions throughout both structures for the arbitrary (Figs. 17a and b) and box (Figs. 17c and d) beams. FSO optimization utilizes the majority of the shell geometry by setting the shell thickness at the high value of 6 mm. Only in the rear part of the new structure does the shell geometry remain almost without the material (Fig. 17). Owing to the great employment of the shell areas and shell thickness, the new monocoque structure possesses the heaviest weight (100.9 kg) of all of the BSTs achieved.

Considering the total resultant compliance (invert stiffness), the monocoque made of steel displays a notably lower stiffness (compliance: 5540 kNmm for the arbitrary and 5938 kNmm for the box beams) than the other BSTs presented, such as the uni-body. This remark can be explained by the poor load-bearing capability for the load case of bending on the rear axle (1917 kNmm for the arbitrary and 2401 kNmm for the box beams). To overcome this local insufficient stiffness, the automotive industry designs the attached structure of suspension parts as a separate tubular space frame or a separate space frame [9] to [12]. If the term of compliance for bending on the rear axle decreases, the steel monocoque possesses the compliance that is comparable with the other BSTs.

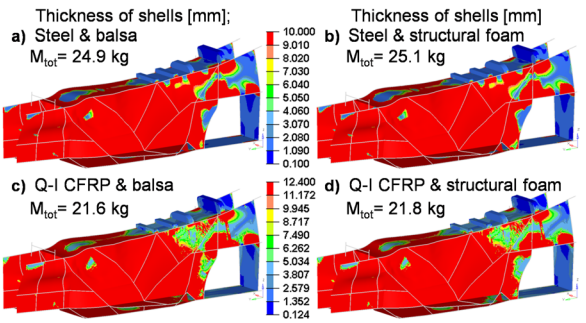

Fig. 18. *ASD results for the monocoque design: a) steel & balsa wood, b) steel & structural foam, c) Q-I CFRP & balsa wood, d) Q-I CFRP & structural foam*

Because of the highest weight of the steel monocoque, we also tested four additional pairs of the lightweight material (material properties from Table 2, [47] to [51]) namely steel with structural foam (AIREX® C70), steel with balsa wood (BALTEK® SB.50), Q-I CFRP with structural foam, and Q-I CFRP with balsa wood. These pairs of the composite sandwich materials were expected to decrease the overall weight of the monocoque structure significantly.

Fig. 18 reports the monocoque designs obtained from the FSO for the four pairs of the lightweight materials and the box beams. These monocoque designs (Fig. 18) display very similar material distributions to the design of the steel monocoque (Fig. 17). The thickness of the shell geometry increases markedly, however, to satisfy the optimization constraints. The thickness of the shells doubles for the Q-I CRFP with the balsa wood and PVC foam.

Owing to the sandwich structure design that offers a notable mass reduction, the monocoque designs of the four material pairs weigh approximately 21.6 kg to 25.1 kg. These weights are comparable with the other BSTs and are considerably less than the unibody design of the shells and box beams. The monocoque designs of the four material pairs exhibit lower stiffness than that of the steel monocoque. If the load-bearing capacity for the loads of the side crash (as a medium value of 2810 kNmm) and bending on the rear axle (as a medium value of 2816 kNmm) increases, the monocoque designs of the four material pairs deliver lightweight and stiff structures.

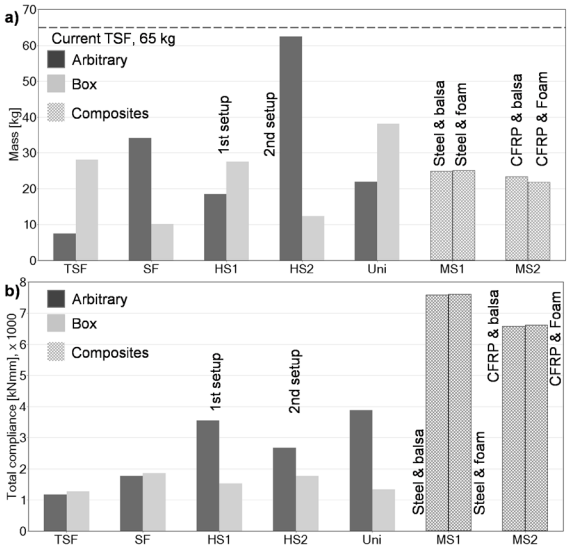

Fig. 19. *Comparison of the resulting BSTs from the ASD application: a) mass level, b) compliance level; TSF tubular space frame, SF space frame, HS hybrid structure, Uni unibody, MS monocoque structure*

These results confirm the original material distribution obtained for the steel monocoque design (Fig. 17) and assert that the ASD also provides worthwhile design suggestions for the monocoque design made of composites (Fig. 18).

As a summary of the ASD's design advantages, Fig. 19 affirms the delivery of the various lightweight design concepts for a new eQuad structure. All of these delivered BSTs present the structural mass (Fig. 19a) that is markedly beneath the current tubular space frame design. The distribution of the total compliance (Fig. 19b) indicates to the stiffest design concepts (Uni, HS1 and TSF) from the obtained BSTs.

4 CONCLUSIONS

In recent years, engineers have begun to apply TO to provide the first design suggestions for new structures. Consequently, TO delivers the bionic shapes that demand additional treatment to obtain manufacturable geometry. Our ASD allows for the smooth transition of the TO results into design concepts of a new structure. The ASD enables engineers to realize the studies of various BSTs within only one FEm by adjusting the model parameters, changing (replacing) available materials and setting the prioritizing of the fundamental structural elements (beams and plates). Our results affirm that the ASD delivers profitable lightweight proposals for the selected BST concepts such as tubular space frame, space frame, hybrid structure, unibody and monocoque.

The ASD results prove that the steering criteria permit engineers to pick and optimize the selected BSTs. Our ASD reveals the characteristics of acting loads such as tension-compression, bending and torsion in the fundamental structural elements (beams and plates) by reporting the cross-sectional parameters (areas and second moments of area) and dimensions of analyzed beams and by pointing out the geometrical shapes as well as thicknesses of additional plates (shells). The ASD results also illustrate the influence of the plate (shell) geometry on the structural stiffness versus the change in the overall weight that can greatly increase the load-bearing of a new structure. Additionally, the ASD results help to identify the acting loads or load cases that provoke the high values of the compliance, which indicates the necessary improvements to increase the structural rigidity (Fig. 19).

Once the design proposals for the possible BSTs are delivered for the new eQuad structure, the most suitable proposal needs to be chosen for the tailoring of a resultant body-in-white step and the further design sophistication phase to take full advantage of real material properties such as strength. Considering our ASD results, the space frame and the second case of the hybrid structure (Fig. 19) assert their advantages over the other BSTs analyzed. The design sophistication phase requires for the final structure refinement that those two chosen BSTs should merge into one coherent design to perform the enhancement of a new tailored structure for real material data. The first results of the design sophistication phase suggest maintaining the level of lightweight design.

5 ACKNOWLEDGEMENTS

This work was accomplished at the VIRTUAL VEHICLE Research Center in Graz, Austria. The authors would like to acknowledge the financial support of K-Project WoodC.A.R. – Computer Aided Research, the COMET K2 - Competence Centers for Excellent Technologies Programme of the Austrian Federal Ministry for Transport, Innovation and Technology (bmvit), the Austrian Federal Ministry of Science, Research and Economy (bmwfw), the Austrian Research Promotion Agency (FFG), the Province of Styria and the Styrian Business Promotion Agency (SFG).

6 REFERENCES

[1] Cavazzuti, M., Baldini, A., Bertocchi, E., Costi, D., Torricelli, E., Moruzzi, P. (2011). High performance automotive chassis design: a topology optimization based approach. *Structural and Multidisciplinary Optimization*, vol. 44, no. 1, p. 45-56, **DOI:10.1007/s00158-010-0578-7**.

[2] Christensen, J., Bastien, C., Blundel, M.V., Grimes, O., Appella, A., Bareham, G., O'Sullivan, K. (2012). Generation of optimised hybrid electric vehicle body in white architecture from a styling envelope. *Global Journal of Researches in Engineering Automotive Engineering*, vol. 12, no. 1.

[3] Agkathidis, A., (2016). Implementing biomorphic design, design methods in undergraduate architectural education. *Proceedings of eCAADe 34th Annual Conference*, vol. 1, p. 291-298.

[4] Rokicki, W., Gawell, E. (2016). Voronoi diagrams – rod structure research models in architectural and structural optimization. *MAZOVIA Regional Studies, Analyses and Studies*, no. 19, p. 155-164, **DOI:10.21858/msr.19.10**.

[5] Galjaard, S., Hofman, S., Perry, N., Ren, S. (2015). Optimizing structural building elements in metal by using additive manufacturing, *Proceedings of International Association for Shell and Spatial Structures Symposium*, Amsterdam.

[6] Fastermann, P. (2014). *3D-Drucken – Wie die generative Fertigungstechnik funktioniert*, Springer Vieweg, Berlin, Heidelberg.

[7] Hagl, R. (2015). Das 3D-Druck-Kompendium, Leitfaden für Unternehmer, *Berater und Innovationstreiber, 2nd Ed.,* Springer Gabler, Wiesbaden, **DOI:10.1007/978-3-658-07047-2**.

[8] Moser, A., Schweiger, R. (2007). Prospects and barriers for Up-Front CAE-Simulation in the automotive development. *Proceedings of NAFEMS World Congress Vancouver*.

[9] Crolla, D.A. (2009). *Automotive Engineering, Powertrain, Chassis System and Vehicle Body*, Elsevier Inc.

[10] Mallick P.K. (2010). *Materials, Design and Manufacturing for Lightweight Vehicles*, Woodhead Publishing Ltd., Cambridge, **DOI:10.1533/9781845697822**.

[11] Davies, G. (2012). *Materials for Automobile Bodies*, Butterworth-Heinemann, Elsevier Ltd., Oxford.

[12] Friedrich, H.E. (2013). *Leichtbau in der Fahrzeugtechnik*, Springer Vieweg, Wiesbaden, **DOI:10.1007/978-3-8348-2110-2**.

[13] Calì, M., Oliveri, S.M., Ambu, R., Fichera, G. (2018). An integrated approach to characterize the dynamic behaviour of a mechanical chain tensioner by functional tolerancing. *Strojniški vestnik - Journal of Mechanical Engineering*, vol. 64, no. 4, p. 245-257, **DOI:10.5545/sv-jme.2017.5079**.

[14] Future Steel Vehicle, Phase 2 - Report (2011). *World Auto Steel*, Brussels.

[15] Hirz, M., Gfrerrer, A., Dietrich, W. (2013). *Integrated Computer-Aided Design in Automotive Development*, Springer-Verlag, Berlin Heidelberg.

[16] Česnik, M., Slavič, J., Boltežar, M. (2016). Assessment of the fatigue parameters from random vibration testing: Application to a rivet joint. *Strojniški vestnik - Journal of Mechanical Engineering*, vol. 62, no. 7-8, p. 471-482, **DOI:10.5545/sv-jme.2016.3774**.

[17] Mršnik, M., Slavič, J., Boltežar, M. (2018). Vibration fatigue using modal decomposition. *Mechanical Systems and Signal Processing*, vol. 98, p. 548-556, **DOI:10.1016/j.ymssp.2017.03.052**.

[18] Höfer, C. (2013). A Winner: Car Body Design Development of the Hyundai Sonata, *Proceedings of 12th annual Great Designs in Steel seminar*, Steel Market Development Institute.

[19] Current & Future Technologies in Automotive Engineering Simulation (CAE) (2008). *AUTOSIM Consortium*, NAFEMS.

[20] Son, I., Noh, Y., Choi, E., Choi, J., Ji, Y., Lim, K. (2018). Optimization of the flow path efficiency in a vacuum cleaner fan. *Strojniški vestnik - Journal of Mechanical Engineering*, vol. 64, no, 4, p. 258-268, **DOI:10.5545/sv-jme.2017.4736**.

[21] Harzheim L. (2014). *Strukturoptimierung: Grundlagen und Anwendungen*, 2. Auflage, Europa-Lehrmittelm.

[22] Kang, B. (2015). CAE for Digital Development. *Proceedings of European Altair Technology Conference*, Paris.

[23] Groth, M. (2015). *Introduction to the theory of derivators*, Mathematical Institute of the University of Bonn, Bonn.

[24] Stanton, M. (2015). Exceeding customer expectations by left shifting with robust virtual engineering at jaguar land rover. *Proceedings of European Altair Technology Conference*, Paris.

[25] Nair, N. (2014). CAE driven multi-disciplinary optimization of vehicle systems. *Proceedings of 13th LS-DYNA Forum*.

[26] The Association of German Engineers (VDI) (1997). *VDI 2221: Methodik zum Entwickeln und Konstruieren technischer Systeme und Produkte*, Verein Deutscher Ingenieure, Düsseldorf.

[27] The Association of German Engineers (1997). *VDI 2222: Blatt 1 Methodisches Entwickeln von Lösungsprinzipien*, Verein Deutscher Ingenieure, Düsseldorf.

[28] Sellgren, U. (1999). *Simulation-Driven Design - Motives, Means, and Opportunities*, PhD Thesis, KTH, Stockholm.

[29] Osborne, G., Prater, G., Lesiv, R., Lamb, D., Castanier, M. (2011). Vehicle concept model abstractions for integrated geometric, inertial, rigid body, powertrain, and FE analyses. *Proceedings of ASME International Mechanical Engineering Congress and Exposition*, Denver, **DOI:10.1115/IMECE2011-63590**.

[30] Steinwall, J., Viippola, P. (2014). *Concept Development of a Light-weight Driver's Seat Structure & Adjustment System*, MSc thesis, Chalmers University of Technology, Gothenburg.

[31] Baskin, D.M., Reed, D.B., Seel, T.N., Hunt, M.N., Oenkal, M., Takacs, Z., Vollmer, A.B. (2008). A Case Study in Structural Optimization of an Automotive Body-In-White Design. *Proceeding of SAE International 2008 World Congress*, Detroit, **DOI:10.4271/2008-01-0880**.

[32] Jedrzejczyk, R.P., Alb, M.S., Jost, T. (2018). Integrative CAE-driven design process in the embodiment design phase of L7e vehicle structures. *Strojniški vestnik - Journal of Mechanical Engineering*, vol. 64, no. 1, p. 3-16, **DOI:10.5545/sv-jme.2017.4489**.

[33] Haberhauer, H., Bodenstein, F. (2014). *Maschinenelemente, Gestaltung, Berechnung, Anwendung, 17th ed*., Springer Vieweg, Berlin Heidelberg, **DOI:10.1007/978-3-642-37417-3**.

[34] Altair Engineering Inc. (2015). *HyperWorks 14.0, OptiStruct Reference Guide*, Troy, Michigan.

[35] Altair Engineering Inc. (2015). *HyperWorks 14.0, OptiStruct User's Guide*, Troy, Michigan.

[36] Parker Steel Company (2016). Metric Size Metals*, Metric Metals Reference Guide*. Toledo.

[37] SSAB (2016). *Structural Hollow Section – Dimensions and Cross-Sectional Properties*, SSAB AB, Stockholm.

[38] Soden, P.D., Hinton, M.J., Kaddour, A.S., (1998). Lamina properties, lay-up configurations for a range of fibre-reinforced compo-site laminates. *Composites Science and Technology*, vol. 58, p. 1011-1022, **DOI:10.1016/S0266-3538(98)00078-5**.

[39] Daniel, M.I., Ishai, O. (2006). *Engineering Mechanics of Composite Materials. 2nd ed*. Oxford University Press, New York, Oxford.

[40] VIRTUAL VEHICLE Research Center (2017). eQuad, from *http://www.v2c2.at/foerderprogramme/k2-forschungsprogramm/ee-software/projects/equad/*, accessed on 2017-10-23.

[41] Edwards, M., Seidl, M., Carroll, J., Nathanson, A. (2014). *Provision of Information and Services to Perform an Initial Assessment of Additional Functional Safety and Vehicle Construction Requirements for L7e-A Heavy On-Road Quads*. Transport Research Laboratory, European Commission, Brussels.

[42] Horvath, C.D., Cannon, M. (2012). Future Material opportunities and direction for lightweighting automotive body structures. *Proceeding of Advanced High-Strength Steels for Automotive Lightweighting USCAR Offices*, Southfield, .

[43] Roland Berger GmbH (2017). *Automotive Metal Components for Car Bodies and Chassis, Global market study*, Munich.

[44] Keeler, S., Kimchi, M., Mooney, P.J. (2017). Advanced High-Strength Steels Application Guidelines Version 6.0, World Auto Steel, Brussels. Jedrzejczyk, R.P., Jost, T. (2015). The finite element assessment of structure properties for an L7e class vehicle under the bending, torsion static and crash loads. *Proceedings of ICoEV International Conference on Engineering Vibration*, Ljubljana.

[45] Malen, D.E. (2011). Fundamentals of Automobile Body Structure Design. *SAE International*, Warrendale, **DOI:10.4271/R-394**.

[46] Jedrzejczyk, R.P., Jost, T. (2015). The finite element assessment of structure properties for an L7e class vehicle under the bending, torsion static and crash loads. *Proceedings of ICoEV International Conference on Engineering Vibration*, Ljubljana.

[47] Songhan Plastic Technology Co., Ltd. (2016). *3A Composites Core Materials BALTEK® SB.50 Structural End-Grain Balsa, Data Sheet*, Fengxian District, Shanghai City.

[48] MatWeb Material Property Data (2018), 3A Composites Core Materials BALTEK® SB.50 Structural End-Grain Balsa, from *http://www.matweb.com/search/datasheet.aspx?matguid=680f7698bfed40d9854a2b2b9ced7c3e&ckck=1*, accessed on 2018-09-18.

[49] Airex AG (2011). *3A Composites Core Materials AIREX® C70 Universal Structural Foam*, Data Sheet, Sins,

[50] MatWeb Material Property Data (2018). 3A Composites Core Materials AIREX® C70.55 Universal Structural Foam, from *http://www.matweb.com/search/DataSheet.aspx?MatGUID=d6bdd351de1240eba63335fb439978e4*, accessed on 2018-09-18.

[51] Stoll, F., Campbell, S., Banerjee, R., Griffin, D. (2008). Blade design with engineered cores materials, *Wind Turbine Blade Workshop*, Albuquerque.